

# Behavior of protruding lateral plane graphene sheets in liquid dodecane: molecular dynamics simulations

Shenghui Chen · Shuangqing Sun · Chunling Li · Charles U. Pittman Jr. · Thomas E. Lacy · Songqing Hu · Steven R. Gwaltney

Received: 23 June 2016 / Accepted: 23 October 2016 / Published online: 7 November 2016  
© Springer Science+Business Media Dordrecht 2016

**Abstract** Molecular dynamics simulations are used to investigate the behavior of two parallel graphene sheets fixed on one edge (lateral plane) in liquid dodecane. The interactions of these sheets and dodecane molecules are studied with different starting inter-sheet distances. The structure of the dodecane solvent is also analyzed. The results show that when the distance between the two graphene sheets is short (less than 6.8 Å), the sheets will expel the dodecane molecules between them and stack together. However, when the distance between two sheets is large (greater than 10.2 Å), the two sheets do not come together, and the dodecane molecules will form ordered layers in the interlayer spacing. The equilibrium distance between the graphene sheets can only take on specific discrete values (3.4, 7.8, and 12.1 Å), because only an integer number of dodecane layers

forms between the two sheets. Once the graphene sheets are in contact, they remain in contact; the sheets do not separate to allow dodecane into the interlayer spacing.

**Keywords** Graphene · Sheets ends · Dodecane · Interaction · Molecular dynamics simulation · Modeling and simulation

## Introduction

Graphene has attracted significant attention due to its unusual electrical, chemical, thermal, and mechanical properties (Novoselov et al. 2004; Lee et al. 2008; Du et al. 2008; Georgakilas et al. 2012; Sadasivuni et al. 2014). Incorporating graphene in composite materials as nanofiller can enhance the mechanical, electrical, and thermal properties of the composites (Kuilla et al. 2010; Huang et al. 2012; Mittal et al. 2015). Graphene-based composites have found applications such as in sensors and high-strength materials (Singh et al. 2011; Hu et al. 2014). Graphene can offer enhanced mechanical properties in polymers when compared to carbon nanotube reinforcements due to graphene's planar structure and high aspect ratio, which offer better stress transfer in a matrix (Zhao et al. 2010; Rafiee et al. 2010).

Uniform and homogeneous dispersion of nanofillers in the matrix has significant effects on the composite properties (Kango et al. 2013; Kuila et al. 2012). The large surface area of graphene results in strong interactions between two graphene sheets, including van der Waals forces and strong  $\pi$ - $\pi$  interactions (Si and

---

S. Chen · S. Sun (✉) · C. Li · S. Hu (✉)  
College of Science, China University of Petroleum (East China),  
Qingdao 266580, People's Republic of China  
e-mail: sunshuangqing@upc.edu.cn  
e-mail: songqinghu@upc.edu.cn

C. U. Pittman Jr., · S. R. Gwaltney  
Department of Chemistry, Mississippi State University,  
Mississippi State, MS 39762, USA

T. E. Lacy  
Department of Aerospace Engineering, Mississippi State  
University, Mississippi State, MS 39762, USA

S. Hu  
Key Laboratory of New Energy Physics & Materials Science in  
Universities of Shandong, China University of Petroleum (East  
China), Qingdao 266580, China

Samulski 2008a, b). Under these strong interactions, graphenes aggregate and stack in the host matrix, which reduces the aspect ratio of the resulting graphite stack and significantly affects the composite's properties. Thus, the performance of graphene-based composites is limited by aggregation and stacking. To obtain better performance from graphene-based composites, it is important to understand the aggregation and interactions of graphene sheets in a host matrix.

Some approaches have been used to reduce the aggregation of graphene in composites. Stankovich et al. (2006) presented a general approach for the preparation of graphene nanosheet (GNS)/polymer composites via reduction of organic modified graphite oxide (GO) nanosheets in the polymer solvent. Wei et al. (2009) used in situ reduction-extractive dispersion technology to prepare the graphene nanosheet/polymer composites. They showed that reduction-extractive dispersion technology can effectively promote the dispersion of graphene nanosheets. Li et al. (2008) reported that chemically converted graphene sheets obtained from graphite can readily form stable aqueous colloids through electrostatic stabilization. This method can be used for large-scale production of aqueous graphene dispersions without polymeric or surfactant stabilizers. Yang et al. (2011) found that multi-walled carbon nanotubes could inhibit the aggregation of multi-sheet graphitic platelets, and synergetic effects between the multi-sheet graphitic platelets and the multi-walled carbon nanotubes could improve the mechanical properties and thermal conductivity of epoxy composites.

Although several methods that can reduce graphene aggregation have been found experimentally, experimental studies of graphene behavior at the atomic level and of aggregation mechanisms are very difficult. Computational simulations have been applied in graphene-based composites (Montazeri and Rafii-Tabar 2011; Ebrahimi et al. 2012; Zhang et al. 2012). To date, most of computational simulations in this area focus on predicting the properties of composites and the interactions between graphene and host molecules. However, simulations of interaction of two graphene sheets and the micro-aggregation behavior of graphene are scarce. Zhang and Jiang (2014) studied the mechanical performance of graphene/graphene oxide paper-based polymer composites using molecular dynamics (MD) simulations. The polymer conformations were found to affect the interlayer spacing between graphene sheets. However, their work also focused on the properties of

composites. The aggregation behavior of graphene sheets and the interaction between them were not further analyzed. An in-depth understanding of the interactions between separated graphene sheets as a function of solvent and of graphene surface chemistry would help to design more stable dispersions. When multilayered graphene aggregates are sheared in a liquid media, deaggregation involves solvation of the separating graphene layers. This deaggregation involves solvent penetration from the lateral (edge) planes of the multilayered nanoparticles. In this respect, very little is known about the molecular details of aggregation or deaggregation behavior when mixing is conducted in a host resin.

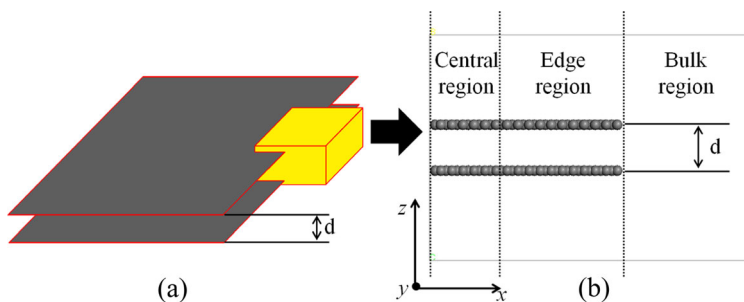
In the present work MD simulations are used to study the micro-behavior of graphenes. Entire graphene sheets or stacked sheets are currently too large to simulate. Therefore, we choose to study uneven ends of graphene sheets, since the ends govern when host molecules enter into or diffuse out of the interlayer spacing. In this work, we constructed simple models of the lateral plane ends of graphene sheets in a liquid dodecane. Then the behavior of the graphene with different initial distances between the graphene sheets was studied where the edges had sheets protruding into the liquid. The interactions between the two graphenes and the dodecane molecules and the effects of the sheets on the dodecane molecules were also analyzed. This work reveals a microscopic view of how unfunctionalized graphene lateral planes might initially behave during deaggregation. It also points out some behavior that is relevant to aggregation in dodecane.

## Calculation models and methods

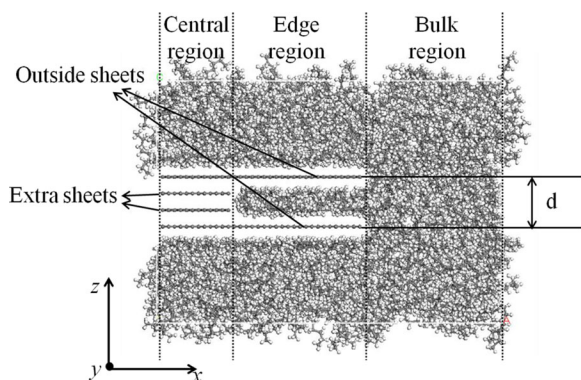
### Simulation model

Figure 1a shows two simplified graphene sheets. In this work we simulate the end portion in the yellow region. Thus, a model of the ends of graphene sheets is obtained that can be separated by various distances (Fig. 1b). The  $z$  direction is chosen perpendicular to the graphene sheets, and the sheets are made continuous in the  $y$  direction. This model includes three regions: the central region, the edge region, and the bulk region. In order to prevent dodecane molecules from entering into the interlayer spacing from the central region, extra graphene sheets (Fig. 2) are

**Fig. 1** View of **a** two real-size sheets and **b** the pure graphene end model built in this work



added in the central region lying between the two outside sheets. The distance between two adjacent graphene sheets (including between the inside sheets and the outside sheets) is 3.4 Å. Filling the rest of the simulation box with dodecane gives the simulation model (Fig. 2). Dodecane was chosen as the solvent as a representative medium- to long-chain liquid hydrocarbon. This work focuses on the behavior of the graphene sheets in the edge region. Thus, the coordinates of the graphene atoms in the central region are fixed, including all atoms of the extra graphene sheets and the atoms of the outside sheets in the central region. Graphene sheets are much larger than a dodecane molecule, so dodecane molecules move far faster than the entire graphene sheets. Graphene edges of the lateral planes are the first parts of all but the basal planes of the surface sheets to interact with dodecane. Thus, adding extra sheets and fixing the graphene carbon atoms in the central region is reasonable. Sheets in the edge region extending into the dodecane are free to bend (see the results in Fig. 2). Thus, the simple models used here are reasonable for examining the behavior of graphene ends.



**Fig. 2** Complete end model simulated in this work

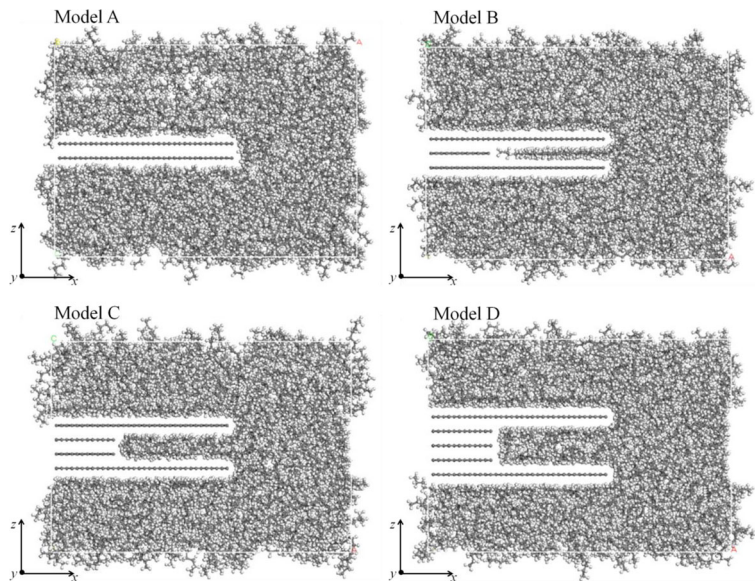
The simulation cell size is  $71.3 \times 42.6 \times 50 \text{ \AA}^3$ , with the origin placed at the bottom left corner of the primary cell. In all models, the lengths of the outer graphene sheets are 40.6 Å, and the lengths of the extra sheets are 13.5 Å. This cell is periodic in the  $x$ ,  $y$ , and  $z$  directions. The distance between graphenes in repeated slabs is at least 36.4 Å (much larger than the cutoff distance, which is 12.5 Å) in the  $x$  and  $z$  directions, in order to prevent spurious interactions between repeated slabs. The graphenes are periodic in the  $y$  direction to simulate large graphene sheets. Four models were built (models A, B, C, and D, shown in Fig. 3) with inter-sheet distances of 3.4, 6.8, 10.2, and 13.6 Å, respectively, by inserting zero, one, two, and three extra inside sheets between the outer sheets. The numbers of atoms for models A to D are 18,342; 18,322; 18,302; and 18,244, respectively.

### Dynamics simulation

The Condensed-Phase Optimized Molecular Potentials for Atomistic Simulation Studies (COMPASS) force field (Sun 1998) was used in the simulations. It is a commonly used, well-calibrated hydrocarbon force field (Wu et al. 2016; Arash et al. 2014; Zheng et al. 2007; Asche et al. 2016). The Ewald method was used for the Coulomb interactions, and the atom-based method with a 12.5 Å cutoff distance was used for the van der Waals interactions. A geometry optimization was carried out for 10,000 iterations using the Smart Minimizer method built into the Materials Studio software package<sup>1</sup> to minimize the total energy. The MD simulations were run in the NVT (constant volume, temperature, and number of particles) ensemble. An MD simulation method similar to that used by Nouranian et al. (2011) and Jang et al. (2012) was employed. First, the MD

<sup>1</sup> Accelrys, Inc. <http://accelrys.com/products/materials-studio/> (date accessed: January 12, 2011)

**Fig. 3** Initial structures of graphene end models. Model A: initial  $d = 3.4 \text{ \AA}$ ; model B: initial  $d = 6.8 \text{ \AA}$ ; model C: initial  $d = 10.2 \text{ \AA}$ ; model D: initial  $d = 13.6 \text{ \AA}$



simulation was run for 2 ps at 10 K. The temperature was then increased to 50 K and then further up to 1000 K in increments of 50 K. At each intermediate temperature, the dynamics simulation was run for 2 ps. A 4-ns dynamics simulation was run at 1000 K to obtain an equilibrated structure. After that, the cell was cooled to 300 K in 50-K decrements, with 2 ps MD simulation runs at each intermediate temperature. Finally, the MD simulation was continued for another 4 ns at 300 K to ensure structure equilibration. All the analyses below were obtained from the last 1 ns of the MD simulations at 300 K. One snapshot every 10 ps was used for the analyses. The same procedure was used for all the model systems.

### Calculating interaction energies

In this work, two types of interaction energies ( $\Delta E$ ) were calculated. One is the interaction energy of all the graphene sheets with dodecane molecules, calculated using Eq. 1 below:

$$\Delta E_{\text{all sheets}} = E_{\text{total}} - (E_{\text{all sheets}} + E_{\text{dodecane}}) \quad (1)$$

where  $E_{\text{total}}$  refers to the total energy of the entire system (graphene sheets plus dodecane molecules).  $E_{\text{all sheets}}$  refers to the energy of all the graphene sheets with no dodecane present.  $E_{\text{dodecane}}$  refers to the energy of all the dodecane molecules with no graphene sheets present.

The second type of interaction energy is the interaction energy of one outside sheet with everything else in the cell, as defined in Eq. 2 below:

$$\Delta E_{\text{one sheet}} = E_{\text{total}} - (E_{\text{one sheet}} + E_{\text{remaining}}) \quad (2)$$

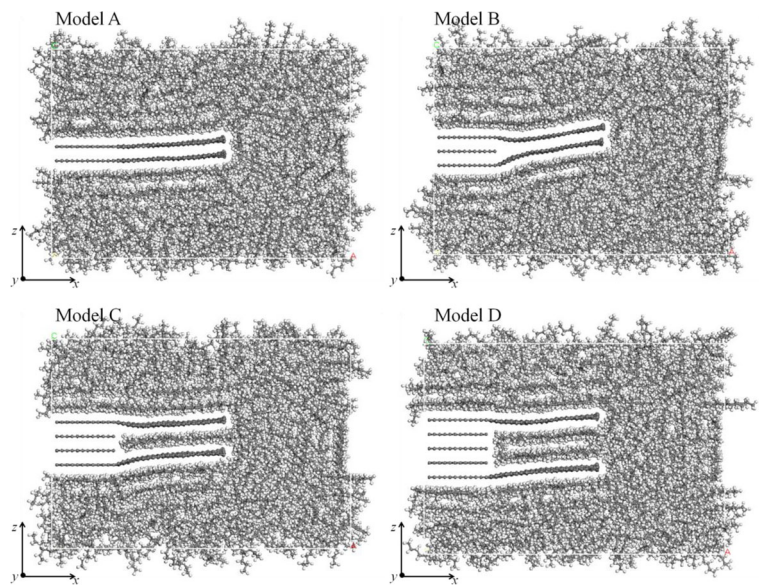
where  $E_{\text{total}}$  again refers to the total energy of the graphene sheets and the dodecane molecules and  $E_{\text{one sheet}}$  refers to the energy of one outside sheet of graphene.  $E_{\text{remaining}}$  refers to the energy of what is left in the simulation cell after removing the one outside sheet from the cell and includes the energies of the other outside sheet, the extra sheets, and all of the dodecane molecules. The  $\Delta E_{\text{one sheet}}$  reported here is the average of the two outside sheets'  $\Delta E_{\text{one sheet}}$ . All structures were frozen during the interaction energy calculations.

## Results and discussion

### Equilibrated structures

The equilibrated structures with different initial interlayer distances between the outside sheets (models A, B, C, and D) are shown in Fig. 4. When the initial interlayer distance is short (3.4 and 6.8  $\text{\AA}$ ), during the MD simulations, the two outside sheets in the edge region stack together, with no dodecane molecules in between. However, for the larger inter-sheet initial distances (models C and D), the two sheets do not come together but stay separated by dodecane molecules. In all four

**Fig. 4** Equilibrated structures of graphene end models. Model A: final  $d = 3.4 \text{ \AA}$ ; model B: final  $d = 3.7 \text{ \AA}$ ; model C: final  $d = 7.8 \text{ \AA}$ ; model D: final  $d = 12.1 \text{ \AA}$



simulations, the outside sheets bend, and the equilibrium distances between the two outside sheets are different from the initial distances. In addition, this equilibrium distance in model D is larger than that in model C and is much larger than those in models A and B (where the outside sheets are in contact, cf. Fig. 4).

The structure of the graphenes

In the equilibrated structures of the four models, the outside sheets in the edge region are almost parallel to the  $y$  axis, and so the average  $z$  coordinates of the atoms in the edge region of one sheet can be used to indicate the position of the sheet in the edge region in the  $z$  direction. Thus, the distance between the two outer sheets in the edge region can be calculated from the differences of the average  $z$  coordinates for the two sheets. These distances are shown in Fig. 5.

In all four equilibrated structures, the interlayer distances between the two outside sheets (the solid lines in Fig. 5) remained stable during the simulations. The two sheets in the edge region shifted up and down together after the model was equilibrated, but the distance between them remained consistent over time. The interlayer distance for model A between the sheets in the edge region is stable at  $3.4 \text{ \AA}$  when the structure is equilibrated, which is the same as the original interlayer distance of graphite,  $3.4 \text{ \AA}$ . The calculated equilibrium interlayer distance for model B between the sheets in the edge region is stable at  $3.7 \text{ \AA}$ . However, from the

equilibrated structure of model B (Fig. 6), we can see that the sheets in the edge region in model B are tilted away from the  $x$  axis. Thus, the nearest contact distance, which is normal to the sheets, is less than the average differences of the  $z$  coordinates. Hence, the actual distance between the two sheets in the edge region is less than the calculated distance of  $3.7 \text{ \AA}$  and is close to the original interlayer distance of graphite,  $3.4 \text{ \AA}$ .

In models A and B, when the initial distance between the sheets is  $6.8 \text{ \AA}$  or shorter, the sheets expel the

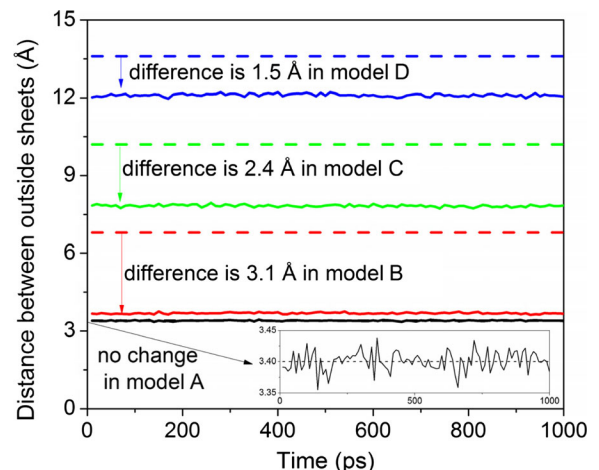


**Fig. 5** The interlayer distance between the outer sheets in the initial structures (dashed lines) and the equilibrated structures (solid lines) for the four models. The amount the sheets approach each other is also shown (see arrows and difference values). Black, red, green, and blue lines are for models A, B, C, and D, respectively

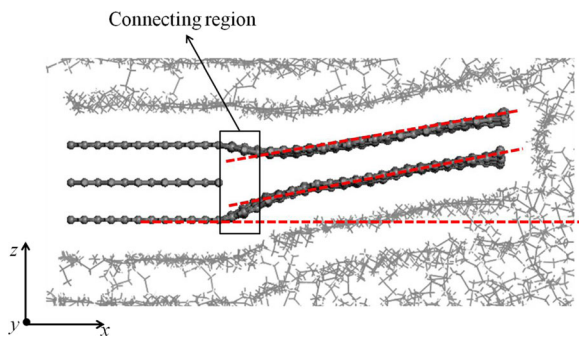


**Fig. 6** The direction of graphene sheets in the edge region in model B

dodecane molecules from within the interlayer spacing, and the two sheets will approach each other (i.e., the sheets “collapse”). This results in the stacking observed, where the sheet spacing closes to 3.4 Å away from the curved portions of the outer sheets near the central region (Fig. 6). Two factors could contribute to the stacking of graphene sheets, the interactions between graphenes, and the interactions among dodecane molecules. It is impossible to determine from the results of this work which is the major driving force. In model B (Fig. 6), the outer sheets are tilted away from the  $x$  axis. This allows the two protruding sheets to get close to one another, while also permitting the sheets to remain flat, which is a lower energy geometry. The connecting region of the two outer sheets (Fig. 6) cannot be flat because the sheets must bend to permit the portions protruding into dodecane to be flat and to be close to each other. If this outer aligned region is not tilted, they must undergo bending along the  $x$  axis, leading a higher energy geometry. The degree of bending required is smaller when tilting away from the  $x$  axis occurs.

The equilibrium interlayer distance in model C changes from the initial distance of 10.2 Å to the equilibrated distance of 7.8 Å (Fig. 4). For model D, the equilibrated distance is even larger; the average distance is 12.1 Å (Fig. 4). In models C and D, the initial separation distance is large (equal to or greater than 10.2 Å), and the sheets remain separated with dodecane molecules staying in the interlayer spacing. Because of the necessarily discrete nature of the interlayer spacings in this study, it is not possible to determine precisely where the interlayer spacing cutoff for sheet aggregation lies and whether the cutoff depends on the length of the edge region.

The extent to which the sheets approach each other is illustrated in Fig. 5. Here, the initial interlayer distances (dashed line) and the difference between the average

distances in the initial and equilibrated structures are shown. The equilibrium distance in model A almost exactly coincides with the initial distance of 3.4 Å. The outer sheets get closer by more than 3.1 Å in model B, with the outer sheet distance decreasing from 6.8 Å to less than 3.7 Å. This distance change in model B is the largest among the four models. The corresponding interlayer distance in model C changes from 10.2 to 7.8 Å, a distance change of 2.4 Å. The distance difference in model D is 1.5 Å, with the outer sheet spacing decreasing from 13.6 to 12.1 Å. In models B, C, and D, the graphene sheets do not stay at their initial positions but get closer to the equilibrium distances through large displacement shifts. Moreover, the distance between the sheets only takes on certain discrete values. These simulations of models B, C, and D revealed three discrete inter-sheet distances of about 3.4, 7.8, and 12.1 Å, respectively. The intervals between these discrete values are almost the same, 4.3–4.4 Å. When the initial distance between the outer sheets is not one of these discrete values, the outer graphene sheets approach each other in order to obtain to one of these preferred values.

To analyze the displacements of the sheets in the  $z$  direction, the average  $z$  coordinates of all the atoms in the edge regions of both outside sheets were calculated for the four models (Fig. 7). The sheets in the four models are observed to vibrate slightly in the  $z$  direction after equilibration. However, the average  $z$  coordinates remain stable at 26.0, 27.1, 26.0, and 26.1 Å, respectively. The average  $z$  coordinate of the sheets for model B is larger than for the others, because the sheets in the edge region shift further away from their original position (Fig. 6).

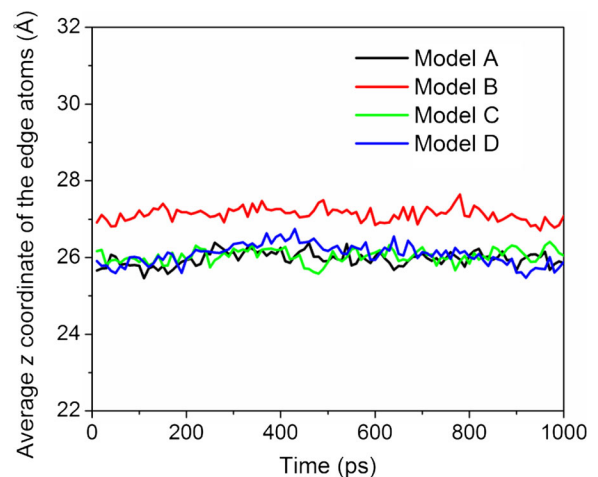


**Fig. 7** The average  $z$  coordinates of the atoms in the edge regions of the outer graphene sheets for the four models

### The configuration of the dodecane molecules

To analyze the distribution of dodecane molecules in the edge region, relative dodecane concentration profiles in the  $z$  direction were generated for the four models (Fig. 8). The relative concentration profiles were shifted in the  $z$  direction to place the center of the sheets at  $z = 25.0 \text{ \AA}$  for ease of comparison. Model A shows several peaks and troughs in the concentration profile. This indicates that the dodecane formed several layers parallel to the sheets. This structuring of the dodecane outside the sheets can also be seen in Fig. 4. No dodecane molecules are in the interlayer spacing, so the concentration is zero between 22.875 and 28.625  $\text{\AA}$ , which is the space occupied by the graphene sheets. The relative dodecane concentration profile of model B is similar to that of model A. The graphene sheets occupy the middle, where the concentration is almost zero. However, the peaks and valleys in model B are less prominent than those in model A because of the tilt of sheets in model B (Fig. 6).

The model C concentration profile contains one obvious peak between sheets. Thus, only one layer of dodecane forms in the interlayer spacing, in addition to the clear structuring of the dodecane outside the sheets. Model D has two peaks between sheets (at around 22.5 and 27.5  $\text{\AA}$ ), indicating that two layers of dodecane form between sheets. From models C and D, one can observe that when dodecane molecules form layers in the inter-sheet spaces, only an integral number of layers can be formed in the interlayer spacing between the sheets. This explains why the average distances between sheets only take on the observed specific values. The distances between the sheets are 3.4  $\text{\AA}$  for direct contact between the sheets and 7.8 and 12.1  $\text{\AA}$  for one and two dodecane layers, respectively, forming between the sheets. The interval between the three values is about 4.4  $\text{\AA}$ , which means the thickness of each dodecane layer formed between the sheets is about 4.4  $\text{\AA}$ .

The structure of the dodecane layers formed between the graphene sheets in model C is shown in Fig. 9. The dodecane forms a single molecular layer, which lies flat

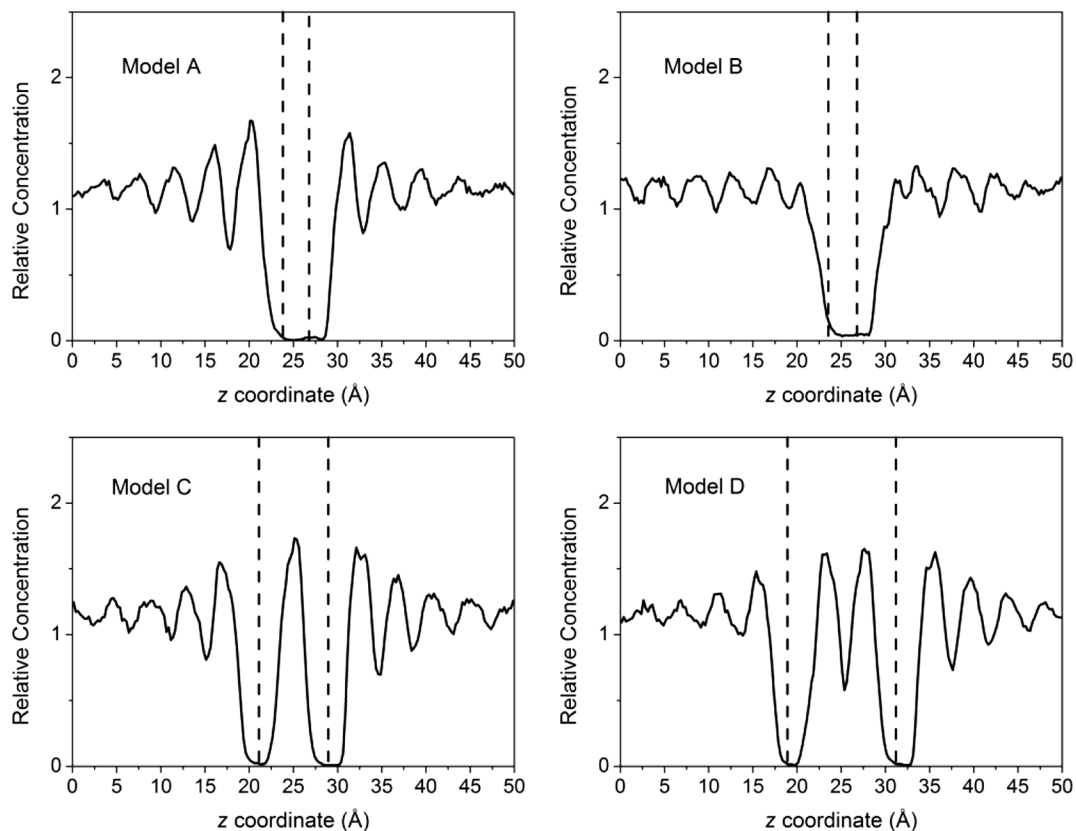


**Fig. 8** Relative concentration profiles for the dodecane in the edge regions for the four models. The *dashed lines* indicate the average  $z$  coordinate for each outside sheet in the edge region

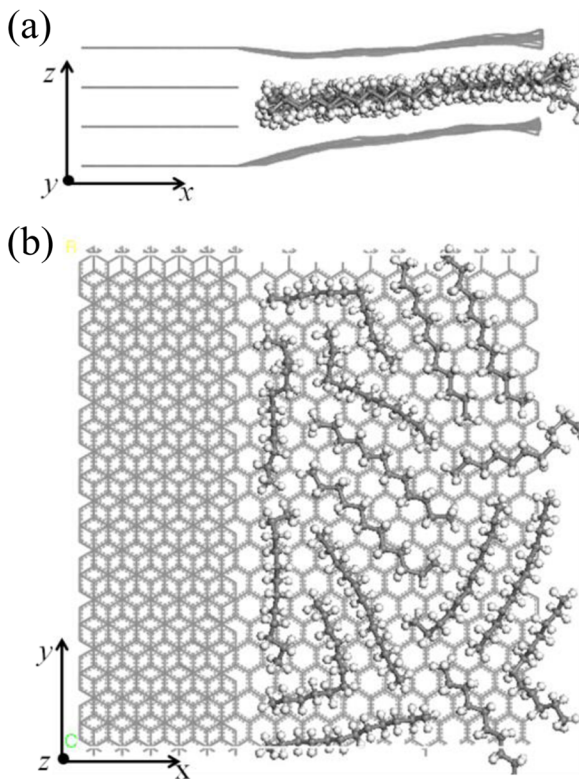


**Fig. 9** A snapshot of the dodecane layer formed between sheets in model C. **a** Side view. **b** Top view. The other atoms are hidden

on the sheets. The van der Waals distances for a dodecane molecule (Fig. 10) are 4.9 and 4.2 Å in the two directions perpendicular to the primary molecular axis. These match well with the thickness of the dodecane layers (4.4 Å) formed between sheets. This also supports the assertion that this single inter-sheet layer is formed by one layer of dodecane molecules lying flat on the sheets. The same sorts of results are obtained when considering model D (Fig. 11).

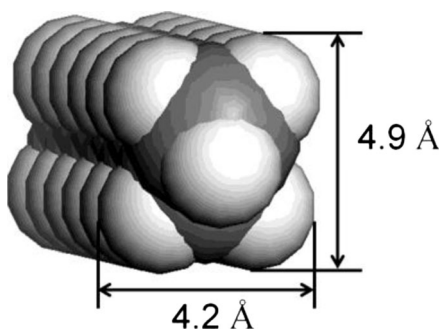


**Fig. 10** The van der Waals thicknesses of a single dodecane molecule in the two directions perpendicular to the primary molecular axis

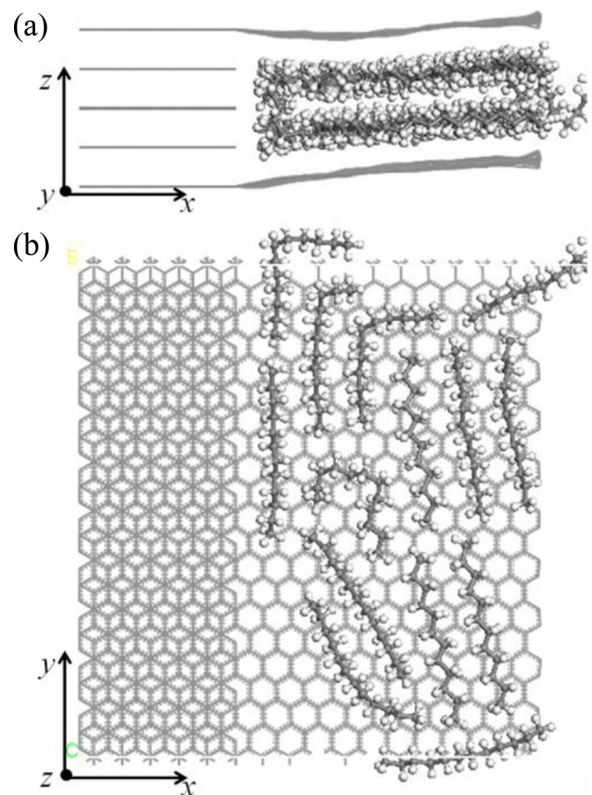


**Fig. 11** A snapshot of one of the dodecane layers formed between sheets in model D. **a** Side view. **b** Top view. The other atoms are hidden

### Interaction energies and binding energies

In order to analyze the interaction strength between graphene and dodecane molecules, two kinds of interaction energies were calculated. The  $\Delta E_{\text{all sheets}}$  in Table 1 is the interaction energy between all the graphene sheets in the box and the dodecane molecules. The  $\Delta E_{\text{one sheet}}$  in Table 1 is the average (of the two)  $\Delta E_{\text{one sheet}}$  interaction energies between one outside sheet and what is left in the box after removing that one outside sheet.

**Table 1** Interaction energies for all sheets and for one outside sheet for the five models. For the definition of model E, see text

Model	A	B	C	D	E
$\Delta E_{\text{all sheets}}$ (kcal/mol)	-1238.0	-1278.2	-1794.9	-1899.0	-1312.6
$\Delta E_{\text{one sheet}}$ (kcal/mol)	-1218.0	-1145.3	-906.2	-881.1	-1076.8



The  $\Delta E_{\text{all sheets}}$  values in Table 1 are similar in models A and B. This is because the structures in models A and B are similar, with the sheets in contact in both. Also, the  $\Delta E_{\text{all sheets}}$  values are roughly similar in models C and D, because the sheet structures in models C and D are both separated.

In Table 1,  $\Delta E_{\text{all sheets}}$  in models A and B are smaller than those in models C and D. In models C and D, dodecane molecules are in the interlayer spacing between the sheets, and the total surface area where graphene is in contact with dodecane is substantially larger in models C and D than in models A and B, which leads to approximately 50 % larger interaction energies in models C and D.

On the other hand,  $\Delta E_{\text{one sheet}}$  in models A and B are larger than those in models C and D. In models A and B, the outside graphene sheets are in contact with dodecane on one side, while the other side is in contact with the other outer graphene sheet because the sheets are together with no dodecane molecules between them. However, in models C and D, the outside graphene sheets in the edge region are in contact with dodecane molecules on both sides. Thus, based on the  $\Delta E_{\text{all sheets}}$  and  $\Delta E_{\text{one sheet}}$  data for models A and B versus those for models C and D, we conclude that the energetically most favorable arrangement of the systems maximizes the graphene-graphene interactions, while also maximizing the dodecane-dodecane interactions. However, these data are not adequate to determine whether the graphene interactions or the dodecane interactions are the driving force for graphene sheet aggregation.

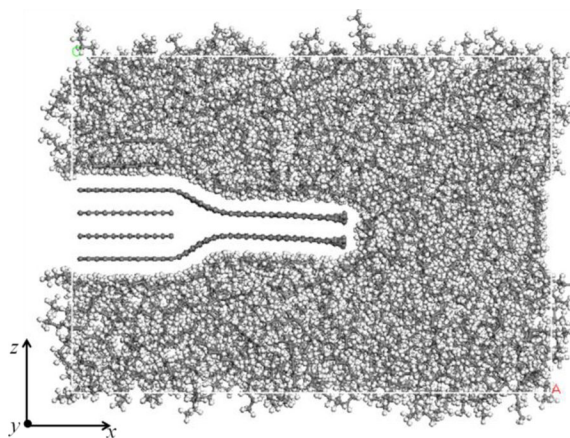
The binding energies of the outer graphene sheets were calculated to analyze the interaction between graphene sheets. The binding energies for models A to D are 598.3, 516.5, 174.4, and 44.9 kcal/mol, respectively. The binding energy decreases obviously with the increase of initial interlayer distance. Model B's binding energy is only 81.8 kcal/mol smaller than that of model A, since the structures in model A and B are similar where the outside graphene sheets in the edge area are in contact with each other. The small decrease between models A and B is due to the bending of graphene sheets in the connecting region in model B. The binding energy of models C is much smaller, because the outer sheets in models C are not contacted directly. In model D, the equilibrium interlayer distance is largest, 12.1 Å, leading to the smallest binding energy.

## The pre-contact sheet model

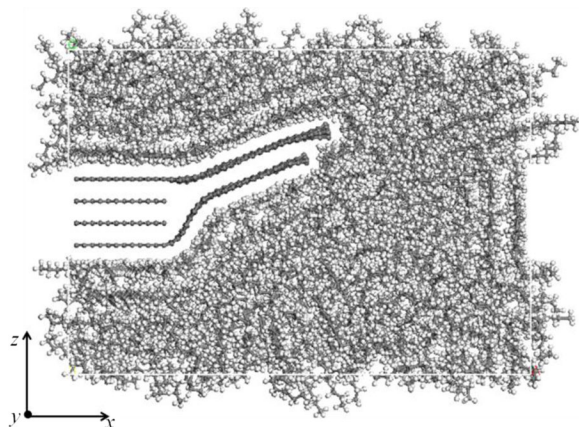
Some dodecane molecules still remain in the interlayer spacing in model C (in Fig. 4) after the MD simulation. Will dodecane diffuse into the interlayer spacing if no dodecane molecules are present between the sheets in the initial structure? To investigate this question, we built a pre-contact sheet model (model E, Fig. 12) as an initial structure, in which the initial outside sheets in the edge region are closed together with no dodecane molecules between them. Model E was built by optimizing the graphene sheets in the absence of dodecane and then adding dodecane afterwards.

Figure 13 shows the equilibrated structure for model E. The dodecane molecules do not separate the graphene ends and so do not diffuse into the interlayer spacing. The sheets in the edge region remain in contact with each other in the equilibrated structure. The outer sheets are tilted away from the  $x$  axis in the equilibrated structure to allow the graphene sheets to be relatively flat and to be close to each other simultaneously. This is the same behavior exhibited with model B and was explained earlier.

We also calculated  $\Delta E_{\text{all sheets}}$ ,  $\Delta E_{\text{one sheet}}$  (Table 1), and binding energy for model E. The  $\Delta E_{\text{all sheets}}$  value for model E is consistent with those for models A and B, since model E has no dodecane in the interlayer space. The lower  $\Delta E_{\text{one sheet}}$  value for model E (−1076.8 kcal/mol), compared to those for models A (−1218.0 kcal/mol) and B (−1145.3 kcal/mol), presumably arises from the strain caused by the substantial bending of the graphene sheets in model E. On the other hand,  $\Delta E_{\text{all sheets}}$  for model E (−1312.6 kcal/mol) is smaller than that of model C (−1794.9 kcal/mol), because in model C the sheets interact with the interlayer dodecane molecules. The  $\Delta E_{\text{one sheet}}$  in



**Fig. 12** Initial structure of the pre-contact model (model E)



**Fig. 13** Equilibrated structure of the pre-contact model (model E)

model E ( $-1076.8$  kcal/mol) is larger than that of model C ( $-902.2$  kcal/mol), because the interactions are stronger when the two graphene sheets are in contact. This is consistent with the analysis in “Interaction energies and binding energies” section. The binding energy for outer sheets in model E is  $488.3$  kcal/mol, which is much larger than that for model C ( $174.4$  kcal/mol). This large increase arises from the direct contact between the outer sheets in the edge area.

Comparing the results of model C to that of model E, we see that when dodecane starts between the sheets, the interactions between the sheets are not strong enough to expel the dodecane on the 10-ns timescale of these simulations. Meanwhile, when the sheets are in contact with each other, the dodecane molecules do not diffuse between or separate the sheets on the timescale of these simulations, either. Both model C and model E are metastable configurations. Entropy favors the sheets being in contact, because of the extra translational, rotational, and conformational freedom enjoyed by dodecane molecules in bulk when compared to dodecane molecules in a monolayer between the sheets. Additionally, enthalpy appears to favor maximizing graphene-graphene and dodecane-dodecane interactions. These imply that model E should have a lower free energy. However, the barrier for interconversion between the presence of a dodecane monolayer (model C) and the sheets being in contact (model E) must be quite large, as evidenced by the lack of interconversion even at 1000 K.

To analyze the binding strength of outer sheets, the binding energy for model E was also calculated.

The binding energy for outer sheets in model E is  $488.3$  kcal/mol, which is much larger than that for model C ( $174.4$  kcal/mol). This large increase arises from the direct contact between the outer sheets in the edge area.

## Conclusions

In the present work, we performed MD simulations of the behavior of two graphene sheets that protrude from the edge of graphene nanostacks in the presence of liquid dodecane. The interactions of these sheets and dodecane molecules are studied with different starting inter-sheet distances. The structure of the dodecane solvent is also analyzed. When the distance between two graphene sheets is short (less than  $6.8$  Å), the sheets can expel the dodecane molecules between them and aggregate. However, when the distance between two sheets is large (greater than  $10.2$  Å), the interaction between two sheets is not strong enough to push out the dodecane molecules, and the dodecane molecules form layers in the spacing between the sheets.

The average distance between the graphene sheets can only take on specific discrete values, because only an integer number of dodecane layers can form between the sheets. The interval between the discrete values is around  $4.4$  Å, because the thickness of a single dodecane layer is around  $4.4$  Å. Finally, if the graphene sheets are in contact with each other, the dodecane molecules will not separate them and diffuse into the interlayer spacing because of the strong graphene-graphene and dodecane-dodecane interactions.

Finally, this modeling methodology would be interesting to apply to other solvents interacting with graphene. For example, the nonpolar aromatic solvents benzene and naphthalene with the ability to interact with both the graphene sheets and themselves via  $\pi$ - $\pi$  stacking interactions represent a particularly interesting case for future studies.

**Acknowledgments** This work is supported by the National Natural Science Foundation of China (51501226) and the Fundamental Research Funds for the Central Universities (15CX08009A, 15CX02066A, and 14CX02221A). We wish to thank the High Performance Computing Collaboratory (HPC<sup>2</sup>) at Mississippi State University for computer time.

## References

- Arash B, Wang Q, Varadan VK (2014) Mechanical properties of carbon nanotube/polymer composites. *Scientific Reports* 4: 6479. doi:10.1038/srep06479
- Asche TS, Behrens P, Schneider AM (2016) Validation of the COMPASS force field for complex inorganic–organic hybrid polymers. *J Sol-Gel Sci Technol*. doi:10.1007/s10971-016-4185-y
- Du X, Skachko I, Barker A, Andrei EY (2008) Approaching ballistic transport in suspended graphene. *Nat Nanotechnol* 3:491–495. doi:10.1038/nnano.2008.199
- Ebrahimi S, Ghafoori-Tabrizi K, Rafii-Tabar H (2012) Multi-scale computational modelling of the mechanical behaviour of the chitosan biological polymer embedded with graphene and carbon nanotube. *Comp Mater Sci* 53:347–353. doi:10.1016/j.commat.2011.08.034
- Georgakilas V, Otyepka M, Bourlinos AB, Chandra V, Kim N, Kemp KC et al (2012) Functionalization of graphene: covalent and non-covalent approaches, derivatives and applications. *Chem Rev* 112(11):6156–6214. doi:10.1021/cr3000412
- Hu K, Kulkarni DD, Choi I, Tsukruk VV (2014) Graphene-polymer nanocomposites for structural and functional applications. *Prog Polym Sci* 39:1934–1972. doi:10.1016/j.progpolymsci.2014.03.001
- Huang X, Qi X, Boey F, Zhang H (2012) Graphene-based composites. *Chem Soc Rev* 41:666–686. doi:10.1039/C1CS15078B
- Jang C, Nouranian S, Lacy TE, Gwaltney SR, Toghiani H, Pittman CU Jr (2012) Molecular dynamics simulations of oxidized vapor-grown carbon nanofiber surface interactions with vinyl ester resin monomers. *Carbon* 50: 748–760. doi:10.1016/j.carbon.2011.09.013
- Kango S, Kalia S, Celli A, Njuguna J, Habibi Y, Kuma R (2013) Surface modification of inorganic nanoparticles for development of organic–inorganic nanocomposites—a review. *Prog Polym Sci* 38:1232–1261. doi:10.1016/j.progpolymsci.2013.02.003
- Kuila T, Bose S, Mishra AK, Khanra P, Kim NH, Lee JH (2012) Chemical functionalization of graphene and its applications. *Prog Mater Sci* 57:1061–1105. doi:10.1016/j.pmatsci.2012.03.002
- Kuilla T, Bhadra S, Yao DH, Kim NH, Bose S, Lee JH (2010) Recent advances in graphene based polymer composites. *Prog Polym Sci* 35:1350–1375. doi:10.1016/j.progpolymsci.2010.07.005
- Lee C, Wei XD, Kysar JW, Hone J (2008) Measurement of the elastic properties and intrinsic strength of monolayer graphene. *Science* 321:385–388. doi:10.1126/science.1157996
- Li D, Müller MB, Gilje S, Kane RB, Wallace GG (2008) Processable aqueous dispersions of graphene nanosheets. *Nat Nanotechnol* 3:101–105. doi:10.1038/nnano.2007.451
- Mittal G, Dhand V, Rhee KY, Park S-J, Lee WR (2015) A review on carbon nanotubes and graphene as fillers in reinforced polymer nanocomposites. *J Ind Eng Chem* 21:11–25. doi:10.1016/j.jiec.2014.03.022
- Montazeria A, Rafii-Tabar H (2011) Multiscale modeling of graphene- and nanotube-based reinforced polymer nanocomposites. *Phys Lett A* 375:4034–4040. doi:10.1016/j.physleta.2011.08.073
- Nouranian S, Jang C, Lacy TE, Gwaltney SR, Toghiani H, Pittman CU Jr (2011) Molecular dynamics simulations of vinyl ester resin monomer interactions with a pristine vapor-grown carbon nanofiber and their implications for composite interphase formation. *Carbon* 49: 3219–3232. doi:10.1016/j.carbon.2011.03.047
- Novoselov KS, Geim AK, Morozov SV, Jiang D, Zhang Y, Dubonos SV et al (2004) Electric field effect in atomically thin carbon films. *Science* 306:666–669. doi:10.1126/science.1102896
- Rafiee MA, Lu W, Thomas AV, Zandiatashbar A, Rafiee J, Tour JM et al (2010) Graphene nanoribbon composites. *ACS Nano* 4:7415–7420. doi:10.1021/nn102529n
- Sadasivuni KK, Ponnamma D, Thomas S, Grohens Y (2014) Evolution from graphite to graphene elastomer composites. *Prog Polym Sci* 39:749–780. doi:10.1016/j.progpolymsci.2013.08.003
- Si Y, Samulski ET (2008a) Synthesis of water soluble graphene. *Nano Lett* 8:1679–1682. doi:10.1021/nl080604h
- Si Y, Samulski ET (2008b) Exfoliated graphene separated by platinum nanoparticles. *Chem Mater* 20:6792–6797. doi:10.1021/cm801356a
- Singh V, Joung D, Zhai L, Das S, Khondaker SI, Seal S (2011) Graphene based materials: past, present and future. *Prog Mater Sci* 56:1178–1271. doi:10.1016/j.pmatsci.2011.03.003
- Stankovich S, Dikin DA, Dommett GHB, Kohlhaas KM, Zimney EJ, Stach EA et al (2006) Graphene-based composite materials. *Nature* 442:282–286. doi:10.1038/nature04969
- Sun H (1998) COMPASS: an ab initio force-field optimized for condensed-phase applications: overview with details on alkane and benzene compounds. *J Phys Chem B* 102:7338–7364. doi:10.1021/jp980939v
- Wei T, Luo G, Fan Z, Zheng C, Yan J, Yao C et al (2009) Preparation of graphene nanosheet/polymer composites using in situ reduction extractive dispersion. *Carbon* 47:2290–2299. doi:10.1016/j.carbon.2009.04.030
- Wu TT, Xue QZ, Li XF, Tao YH, Jin YK, Ling CC, Lu SF (2016) Extraction of kerogen from oil shale with supercritical carbon dioxide:molecular dynamics simulations. *J of Supercritical Fluids* 107:499–506. doi:10.1016/j.supflu.2015.07.005
- Yang SY, Lin WN, Huang YL, Tien HW, Wang JY, Ma CCM et al (2011) Synergetic effects of graphene platelets and carbon nanotubes on the mechanical and thermal properties of epoxy composites. *Carbon* 49:793–803. doi:10.1016/j.carbon.2010.10.014
- Zhang J, Jiang D (2014) Molecular dynamics simulation of mechanical performance of graphene/graphene oxide paper based polymer composites. *Carbon* 67:784–791. doi:10.1016/j.carbon.2013.10.078

- Zhang T, Xue Q, Zhang S, Dong M (2012) Theoretical approaches to graphene and graphene-based materials. *Nano Today* 7: 180–200. doi:[10.1016/j.nantod.2012.04.006](https://doi.org/10.1016/j.nantod.2012.04.006)
- Zhao X, Zhang Q, Chen D, Lu P (2010) Enhanced mechanical properties of graphene-based poly(vinyl alcohol) composites. *Macromolecules* 43:2357–2363. doi:[10.1021/ma902862u](https://doi.org/10.1021/ma902862u)
- Zheng QB, Xue QZ, Yan KY, Hao LZ, Li Q, Gao XL (2007) Investigation of molecular interactions between SWNT and polyethylene/polypropylene/polystyrene/polyaniline molecules. *J Phys Chem C* 111:4628–4635. doi:[10.1021/jp066077c](https://doi.org/10.1021/jp066077c)